JOURNAL OF CATALYSIS **176,** 204–214 (1998)
ARTICLE NO. CA982024

Kinetics and Mechanism of the Reduction of NO by n-Octane over Pt/Al_2O_3 under Lean-Burn Conditions

R. Burch,[1] P. Fornasiero, and T. C. Watling

Catalysis Research Centre, Chemistry Department, University of Reading, Whiteknights, Reading RG6 6AD, United Kingdom

Received October 17, 1997; revised January 15, 1998; accepted January 19, 1998

The effect of temperature, contact time, and reactant concentration on the reduction of NO by n-C_8H_{18} over Pt/Al_2O_3 under oxidising conditions was investigated. The oxidation of n-C_8H_{18} appears to be delicately balanced between two kinetic regimes. At low [C_8H_{18}]/[O_2] the coverage of oxygen on the Pt surface is high, while that of carbonaceous species is negligible, resulting in hydrocarbon oxidation being inhibited by oxygen and in the oxidation of NO to NO_2. At higher [C_8H_{18}]/[O_2] the surface is saturated with carbonaceous species, while the coverage of oxygen is negligible, resulting in hydrocarbon oxidation being zero order in hydrocarbon concentration and in no NO_2 formation being observed. The state of the Pt surface affects the mechanism of NO_x reduction. Thus, NO_x reduction via dissociation of NO on the Pt surface is favoured by a high coverage of carbonaceous species, while a high coverage of oxygen favours NO_x reduction by reaction between n-C_8H_{18}-derived species and spilt-over NO_2 on the Al_2O_3 support and/or metal–support interface. Separate kinetic models capable of fitting the data in these two regions have been developed.

1. INTRODUCTION

The three-way catalyst is very effective in simultaneously removing nitric oxides (NO_x), hydrocarbons, and carbon monoxide (CO) from the exhaust of conventional petrol engines, but requires the air/fuel ratio to be close to the stoichiometric value (1). The new challenge in the automotive pollution control is to also reduce CO_2 emissions. Lean-burn engines offer improved fuel efficiency and, hence, lower CO_2 emissions. However, the exhaust from these engines is strongly oxidising and under these conditions three-way catalysts are no longer effective for NO_x removal. Therefore a new type of catalyst for NO_x control must be developed. One possible catalyst is platinum supported on alumina. Supported Pt catalysts have been found to exhibit high activity and to be both (hydro)thermally stable and resistant to SO_2 (2, 3).

Despite the large number of papers published on the reduction of NO_x under oxidising conditions, the reaction mechanism is still a matter of debate. The main mechanisms proposed can be summarised as followed: (i) oxidation of NO to NO_2 which then reacts with hydrocarbons (4, 5, 6); (ii) formation of highly reactive partially oxidised hydrocarbon intermediate (2, 7); (iii) formation of an isocyanate (–NCO) intermediate (8); and (iv) reduction of the metal surface followed by NO dissociation on the metal (9), possibly with the NO dissociation being assisted by other adsorbed species (10). Other workers have proposed various combinations of these mechanisms. Moreover, Inaba *et al*. (11) have suggested the presence of a co-operative effect between Pt and alumina in the C_3H_8–NO–O_2 reaction. A recent detailed kinetic study has suggested that the reaction mechanism can be different depending on the reductant used (12). It has been proposed that using C_3H_8 or C_3H_6 the platinum surface coverage under the reaction conditions employed is completely different, resulting in different mechanisms for NO reduction. In the presence of C_3H_6 the Pt seems to be in a reduced state and covered with carbonaceous species while in the presence of C_3H_8 the catalyst appears to be oxidised so that the metal is covered with adsorbed oxygen.

Higher hydrocarbons have been shown to be very promising reducing agents, producing high NO_x conversions at relatively low temperatures (90% NO_x conversion at 215°C) and therefore we have decided to study the n-C_8H_{18}–NO–O_2 reaction. The aim of this work is to evaluate the effects of n-C_8H_{18}, NO, and O_2 concentration on the activity and selectivity of Pt/Al_2O_3 for NO_x reduction under lean-burn conditions and hence to gain insight into the reaction mechanism.

2. EXPERIMENTAL

The catalyst used in this study was a standard commercially available 0.3% Pt/Al_2O_3 (CK303, Akzo Chemie). The metal dispersion was measured by H_2 chemisorption at 24°C after reduction in H_2 at 300°C for 0.5 h and degassing at the same temperature for 1 h. The metal dispersion was calculated by back-extrapolating the linear part of the adsorption isotherm (4–11 Torr) to zero and assuming a chemisorption stoichiometry H : Pt = 1 : 1.

[1] Corresponding author. E-mail: R.Burch@reading.ac.uk.

0021-9517/98 $25.00

Catalyst testing was carried out using a quartz tubular downflow reactor (ID 5 mm). The sample (100 mg, grain size 425–600 μm) was held between plugs of quartz wool. A bed of quartz grains was used upstream from the catalyst as a gas preheater and a thermocouple was located in the centre of the catalyst bed. NO, O_2, and He were fed from independent Krohne mass flow controllers, while n-C_8H_{18} was added into the gas stream using an Instech model 2000 syringe pump. All lines to and from the reactor were trace heated (120°C) to prevent n-C_8H_{18} condensation. The total flow was 200 cm^3 min^{-1}, unless stated otherwise. The NO and NO_x concentrations in the reactor outflow were measured by a Signal series 4000 chemiluminesence NO_x analyser. A Perkin Elmer Autosystem gas chromatograph, equipped with both TCD and FID detectors, was used to analyse CO_2, CO, N_2O, N_2, O_2, H_2O, and n-C_8H_{18}. The chromatograph used a Heysep N column and a molecular sieve 5 A column to separate the components. The ratio N_2 : N_2O formed is subjected to relatively large errors due to the low sensitivity of the TCD detector to these components. However, although this affected the absolute analysis of N_2 and N_2O, the nitrogen balances, which were obtained from the chemiluminescence analysis, were better than 100 ± 5%. No reaction was observed over quartz wool or quartz grains below 500°C. Varying the catalyst grain size (120–250, 250–425, 425–600, and 600–825 μm) had no effect on the results indicating freedom from intra-particle transport limitations.

Before taking measurements, the catalyst was pretreated in the reaction mixture for 12 h at 550°C to remove adsorbed species, to partially eliminate possible residue from the metal precursor and to simulate the ageing of the catalyst. For experiments in which the temperature was varied, the temperature was increased stepwise and held constant at each temperature for at least 30 min prior to taking measurements. To determine the effect of reactant concentration, the concentration of one reactant was varied in a random way while the concentration of the others was kept constant. Before changing the hydrocarbon concentration, the catalyst was heated in a mixture of 5% O_2 in He (200 cm^3 min^{-1}) at 10°C min^{-1} to 550°C and the temperature held for 5 min in order to remove carbonaceous species.

3. RESULTS

The effect of temperature on the n-C_8H_{18}–NO–O_2 reaction over 0.3% Pt/Al_2O_3 is shown in Fig. 1. Note that the hydrocarbon concentration utilized is rather high at 8000 ppm of C. The conversion of n-C_8H_{18} and of NO to N_2 and N_2O start at the same temperature (180°C) and increase with increasing temperature until 100% n-C_8H_{18} conversion is reached. The maximum NO_x conversion is about 90%, and the major product is N_2 (selectivity = 65%). As the temperature is increased further the NO_x conversion decreases and NO_2 formation begins. The conversion of NO to NO_2 reaches a maximum at about 350°C. No CO formation was detected in the temperature range investigated. A similar trend was observed previously for the reaction of C_3H_6–NO–O_2 over both Pt/Al_2O_3 and Pt/SiO_2 (13) and was associated with NO_x reduction occurring via NO dissociation on a reduced Pt surface covered by C_3H_6-derived species.

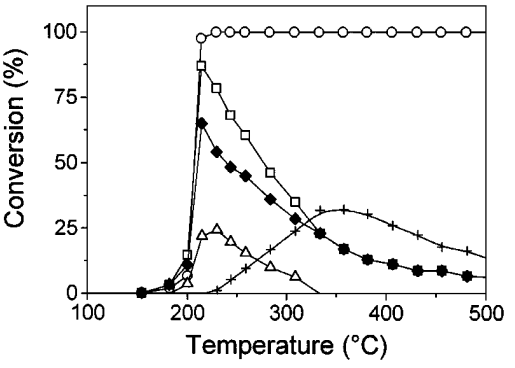

FIG. 1. The effect of temperature on the n-C_8H_{18}–NO–O_2 reaction over Pt/Al_2O_3. Reactant feed: 1000 ppm n-C_8H_{18}, 500 ppm NO, and 5% O_2 (○, n-C_8H_{18}; □, total NO_x; ◆, NO to N_2; △, NO to N_2O; +, NO to NO_2).

Figure 2 shows the effect of hydrocarbon concentration on the turn-over frequency (TOF) of the n-C_8H_{18}–NO–O_2 reaction over Pt/Al_2O_3 at 200°C (all conversions <20%). The platinum dispersion (37%) was measured after the "ageing" pretreatment at 550°C. It should be noted that metal sintering occurs during this process; the fresh sample shows a metal dispersion of 65%. The TOF was calculated as the number of molecules converted per surface Pt atom per unit time. Each point reported in this figure has been taken after 2 h of reaction at the selected concentration. The production of NO_2 has been expressed as a conversion, rather than TOF, since it has been suggested that the

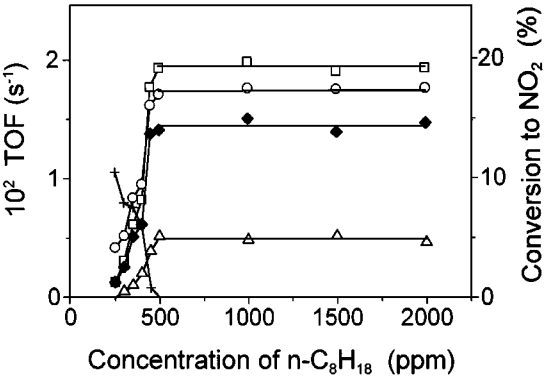

FIG. 2. The effect of varying n-C_8H_{18} concentration on the TOF of n-C_8H_{18} (○), total NO_x (□), NO to N_2 (◆), and NO to N_2O (△), and on the conversion of NO to NO_2 (+) for reaction at 200°C over Pt/Al_2O_3. Reactant feed: 500 ppm NO and 5% O_2.

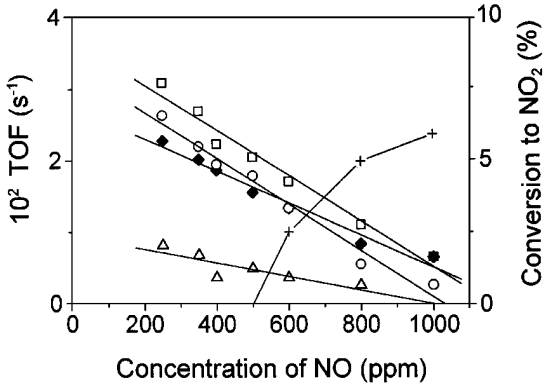

FIG. 3. The effect of varying NO concentration on the TOF of n-C_8H_{18} (○), total NO_x (□), NO to N_2 (◆), and NO to N_2O (△), and on the conversion of NO to NO_2 (+) for reaction at 200°C over Pt/Al_2O_3. Reactant feed: 1000 ppm of n-C_8H_{18} and 5% O_2.

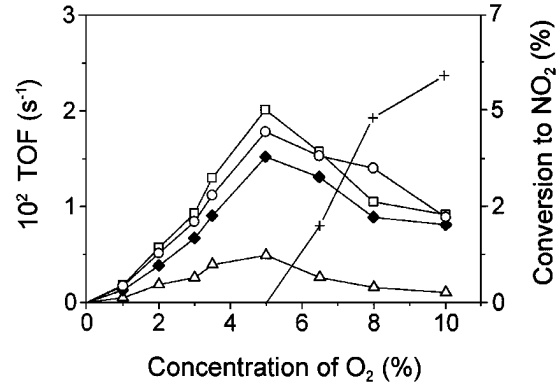

FIG. 4. The effect of varying O_2 concentration on the TOF of n-C_8H_{18} (○), total NO_x (□), NO to N_2 (◆), and NO to N_2O (△), and on conversion of NO to NO_2 (+) for reaction at 200°C over Pt/Al_2O_3. Reactant feed: 1000 ppm n-C_8H_{18} and 500 ppm NO.

rate of NO oxidation to NO_2 is so fast that a pseudo equilibrium is established between NO and NO_2 (This was found to be the case in the C_3H_8–NO–O_2 reaction over Pt/Al_2O_3 (14).) Therefore it is not meaningful to use a TOF for this reaction.

With 500–2000 ppm of n-C_8H_{18} the rates of NO_x reduction and hydrocarbon oxidation are zero order in n-C_8H_{18}. No NO_2 formation was observed in this region. Decreasing the hydrocarbon concentration from 500 to 250 ppm resulted in the TOFs of NO_x reduction and hydrocarbon oxidation decreasing strongly. NO_2 formation was also observed, with the conversion of NO to NO_2 increasing with decreasing hydrocarbon concentration.

The effect of NO concentration on the n-C_8H_{18}–NO–O_2 reaction at 200°C with 1000 ppm of n-C_8H_{18} and 5% O_2 is shown in Fig. 3. With the exception of the NO to NO_2 reaction all rates decrease linearly with increasing NO concentration. Engler *et al.* (15) have observed a similar linear decrease in alkane conversion with increasing NO concentration for the n-$C_{16}H_{34}$–NO–O_2 reaction, while Burch and Watling (14) report the same phenomenon for the C_3H_8–NO–O_2 reaction. At high NO concentration (>500 ppm) NO_2 formation is observed, the conversion of NO to NO_2 increasing with increasing NO concentration.

The effect of varying O_2 concentration at 1000 ppm of n-C_8H_{18} and 500 ppm of NO on the n-C_8H_{18}–NO–O_2 at 200°C is shown in Fig. 4. In the range 0–5% O_2, n-C_8H_{18} oxidation exhibits a high order in O_2 (1.4), suggesting that the coverage of oxygen is small. At higher concentration ($5 < [O_2] < 10\%$) n-C_8H_{18} oxidation is inhibited by O_2. The rate of NO_x reduction follows a similar pattern to the rate of hydrocarbon oxidation. NO_2 formation is observed when the O_2 concentration is greater than 5%.

The effect of temperature, NO and O_2 concentration on the n-C_8H_{18}–NO–O_2 reaction over 0.3% Pt/Al_2O_3 has also been studied with 250 ppm of n-C_8H_{18}, 500 ppm of NO, and 5% O_2 (Fig. 5). Significant conversion of NO to NO_2 was observed starting at about 140°C, before any hydrocarbon conversion occurs. This is in contrast to the case with 1000 ppm of n-C_8H_{18}, where NO_2 was only formed after complete hydrocarbon conversion has occurred. There is a maximum in the conversion of NO to NO_2 of 12% occurring at 170°C which coincides with the beginning of hydrocarbon oxidation. As the temperature is increased further, the conversion of NO to NO_2 decreases and NO_x reduction starts. N_2O production shows a maximum of about 12% at 230°C. At the same temperature the complete conversion of n-C_8H_{18} is reached and the maximum of conversion of NO to N_2 is observed. Under these conditions about 30% of NO is converted to N_2. As the temperature is increased further, conversion of NO to N_2 and N_2O decreases while NO_2 production increases reaching a new maximum at 340°C.

Increasing the NO concentration (Fig. 6) causes the rate of hydrocarbon oxidation to fall, confirming an inhibitory effect of NO on alkane oxidation already observed. Within

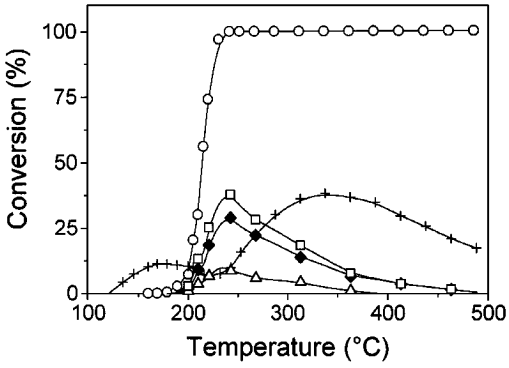

FIG. 5. The effect of temperature on the n-C_8H_{18}–NO–O_2 reaction over Pt/Al_2O_3. Reactant feed: 250 ppm n-C_8H_{18}, 500 ppm NO, and 5% O_2 (○, n-C_8H_{18}; □, total NO_x; ◆, NO to N_2; △, NO to N_2O; +, NO to NO_2).

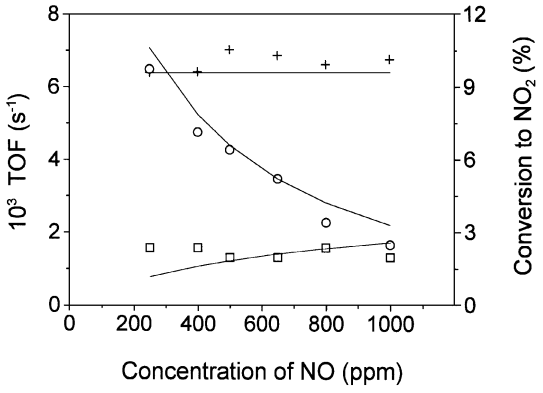

FIG. 6. The effect of varying NO concentration on the TOF of n-C_8H_{18} (○) and total NO_x (□), and on conversion of NO to NO_2 (+) for reaction at 200°C over Pt/Al_2O_3. Lines are fit to low n-C_8H_{18} concentration kinetic model. Reactant feed: 250 ppm n-C_8H_{18} and 5% O_2.

experimental error, the conversion of NO to NO_2 is independent of NO concentration. Increasing O_2 concentration (Fig. 7) results in a decrease in the rate of hydrocarbon oxidation and in an increase in conversion of NO to NO_2. NO_x reduction is approximately zero order in both NO and O_2. The NO_x conversions in Figs. 6 and 7 were too low to enable the amounts of N_2 and N_2O formed to be reliably measured and so these are not shown.

4. DISCUSSION

Before discussing the mechanism of the n-C_8H_{18}–NO–O_2 reaction over Pt/Al_2O_3 we summarise the mechanisms which we have previously proposed for the C_3H_6–NO–O_2 and C_3H_8–NO–O_2 reactions over Pt/Al_2O_3 on the basis of detailed kinetics studies. With C_3H_6, the coverage of C_3H_6-derived species on the Pt surface appears to be high, while the coverage of oxygen is negligible (12). In contrast with C_3H_8, the coverage of oxygen is high and C_3H_8 reacts directly from the gas phase (14). These differences arise from the different reactivity of these reductants with adsorbed oxygen. A consequence of this is that oxidation of NO to NO_2, which presumably requires the presence of adsorbed oxygen on the metal surface, is observed when C_3H_8 is present but not with C_3H_6.

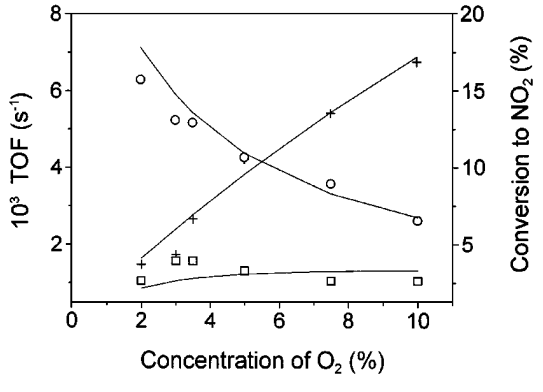

FIG. 7. The effect of varying O_2 concentration on the TOF of n-C_8H_{18} (○) and total NO_x (□), and on conversion of NO to NO_2 (+) for reaction at 200°C over Pt/Al_2O_3. Lines are fit to low n-C_8H_{18} concentration kinetic model. Reactant feed: 250 ppm of n-C_8H_{18} and 500 ppm of NO.

The mechanism of NO_x reduction depends on the state of the surface. With C_3H_6, NO_x reduction appears to occur via dissociation of adsorbed NO to produce adsorbed N which combines with adsorbed N or NO to form N_2 or N_2O. With C_3H_8, NO dissociation does not appear to occur, presumably as a result of the high coverage of oxygen. Instead, NO_x reduction appears to occur on the Al_2O_3 support and/or at the metal–support interface by reaction of C_3H_8-derived species with NO_2, produced by oxidation of NO on the Pt surface. This synergistic model, whereby the main role of the Pt is to produce NO_2 and the role of the alumina is to catalyse the conversion of NO_2 to N_2 has been proposed and elaborated by Hamada and co-workers (11, 16). This model seems well established for systems in which the metal is oxidised and so we shall adopt it for our modelling study for the n-C_8H_{18}–NO–O_2 reaction when the C_8H_{18} : O_2 ratio is low, corresponding to the most oxidising conditions to which the Pt is exposed.

Under some conditions the n-C_8H_{18}–NO–O_2 reaction appears to behave either like the C_3H_6–NO–O_2 or the C_3H_8–NO–O_2 reaction, while under others the behaviour is intermediate between the two. Ideally a single model capable of fitting the data for the whole concentration range would have been developed. However, this has not proved possible. Instead two models have been developed, one for the C_3H_8–NO–O_2 reaction-like region and one for the C_3H_6–NO–O_2 reaction-like region. The justification for developing two separate models is that the state of the Pt surface reflects either a highly reduced or a highly oxidised condition and the kinetics and mechanism of the NO reduction reaction are completely different in the two cases.

In these models it is assumed that all the sites on the Pt surface are equivalent, that there are no adsorbate-adsorbate interactions other than those due to chemical reaction, and that NO adsorption is at equilibrium. The reactor was assumed to exhibit plug flow and transport limitations were assumed to be negligible. The reactor was assumed to behave differentially. The kinetic parameters given in Tables 1 and 2 were determined using the Solver feature of Microsoft Excel 5.0 to vary the parameters to minimise the sum of the square of the differences between experimental and calculated TOFs.

Reaction in the Region $[C_8H_{18}] \leq 250$ ppm, $[NO] \leq 1000$ ppm, $[O_2] \leq 10\%$

For reaction at 200°C with 250 ppm n-C_8H_{18}, the kinetics measured after 2 h exhibit almost exactly the same trends as observed with the C_3H_8–NO–O_2 reaction (14), suggesting

TABLE 1

Parameters Obtained from Fitting the Low C_8H_{18} Concentration Model to Experimental Data

Parameter	Value at 200°C
$k_O K_{O_2}$	3.31×10^2 s^{-1} %$^{-1}$
$k_{C_8H_{18}}$	5.36×10^{-3} s^{-1} ppm^{-1}
K_{NO}	6.12×10^{-2} ppm^{-1}
K_{NO_2}	9.85×10^{-1} ppm^{-1}
k_{NO_x}	4.54×10^{-3} s^{-1}
$k_{NO_2,f}/k_{NO_2,b}$	1.06×10^{-3} ppm^{-1}

that under these conditions the mechanisms of both reactions are similar. Crucial to this is the fact that the Pt surface is highly oxidised so that the only reactions occurring directly on the Pt are combustion of n-C_8H_{18} and oxidation of NO to NO_2. Under these experimental conditions it is possible that the Pt may even be oxidised to PtO_2. However, the precise state of the Pt is less important than the fact that the surface is covered with adsorbed oxygen. The proposed mechanism is summarised in Scheme 1.

n-C_8H_{18} is a saturated molecule and therefore must break a bond to chemisorb on the Pt surface and react. In the literature the rate-determining step of alkane oxidation is generally reckoned to be dissociative chemisorption involving the breaking of a C–H bond (17). In our model the initial step involves the abstraction of a hydrogen (weakly acidic) from the n-C_8H_{18} by an adsorbed O atom (basic site) to give an adsorbed hydroxyl, with the resulting octyl species being bonded to a neighbouring, previously vacant site (Fig. 9). This can be expressed as:

$$C_8H_{18(g)} + O* + * \rightarrow C_8H_{17}* + OH*, \quad k_{C_8H_{18}} C_{C_8H_{18}} \theta_O \theta_V, \qquad [1]$$

where θ_O and θ_V are the fractional coverages of oxygen and vacant sites, $c_{C_8H_{18}}$ is the concentration of n-C_8H_{18}, $k_{C_8H_{18}}$ is a rate constant, and $*$ represents a vacant site. Evidence for this heterolytic C–H bond breaking on a partially oxygen covered Pt surface is given in a recent review (17). Note

TABLE 2

Parameters Obtained from Fitting the High C_8H_{18} Concentration Model to Experimental Data

Parameter	Value at 200°C
$k_N K_{NO}$	4.16×10^0 ppm^{-1} s^{-1}
$2k_{O_2,a}/25$	1.11×10^0 %$^{-1}$ s^{-1}
$k_{NO_2} K_{NO}$	2.39×10^{-1} ppm^{-1} s^{-1}
k_{N_2}	1.20×10^2
K_{NO}	6.12×10^{-2} ppm^{-1}
A	3.77×10^{-2} %$^{-1}$
n	0.590

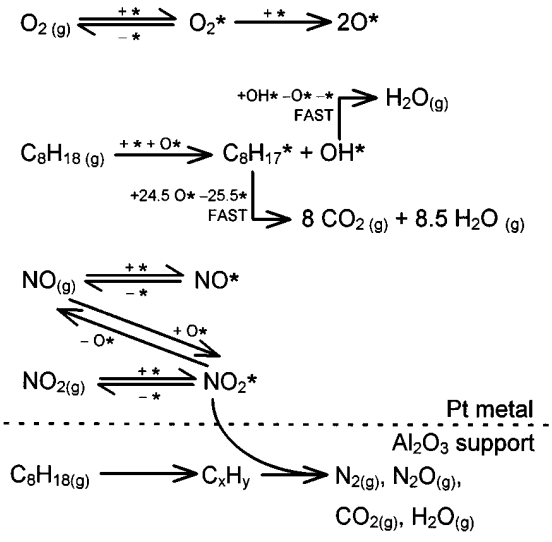

SCHEME 1. Proposed mechanism for the C_8H_{18}–NO–O_2 reaction in the low n-$[C_8H_{18}]/[O_2]$ concentration region. Reactions above the dotted line occur on the Pt surface, while reactions below occur on the Al_2O_3 support.

that Eq. [1] predicts that the rate of n-C_8H_{18} oxidation will be greatest when $\theta_O = \theta_V = 0.5$, which has been observed for the oxidation of CH_4 over Pt catalysts (18). This expression is also consistent with the order in n-C_8H_{18} being greater than unity for $[C_8H_{18}] < 500$ ppm. Under the conditions used here, the reaction is inhibited by O_2, suggesting that $\theta_O > \theta_V$. As the n-C_8H_{18} concentration is increased the rate of removal of adsorbed oxygen from the surface increases, resulting in a fall in θ_O and a corresponding increase in θ_V. This changes the surface coverages towards that required for maximum activity resulting in an increase in the rate of n-C_8H_{18}, in addition to that due to the n-C_8H_{18} term in Eq. [1]; i.e., the order in n-C_8H_{18} is greater than unity, as experimentally observed.

After the initial dissociative adsorption, the adsorbed octyl species reacts rapidly in a series of steps to give CO_2 and surface hydroxyls, which in turn rapidly react to give H_2O. If these steps were not rapid, then a significant coverage of n-C_8H_{18}-derived species and/or hydroxyl groups would build up on the surface inhibiting the reaction and resulting in the order in n-C_8H_{18} being less than unity (in this concentration region). The rapid reaction of the octyl species is in part due to the high surface coverage of oxygen:

$$C_8H_{17}* + 33O* \rightarrow 8CO_{2(g)} + 17OH* + 17* \qquad [2]$$

$$2OH* \rightarrow H_2O_{(g)} + O* + *. \qquad [3]$$

Note that reaction [2] obviously represents a series of reaction steps, rather than a single reaction step.

Oxygen presumably adsorbs dissociatively and irreversibly on the Pt surface; the desorption of adsorbed atomic oxygen is reported to occur only at temperatures

above 400°C (19). The dissociative adsorption of oxygen is assumed to occur in two steps. First, oxygen adsorbs reversibly and molecularly:

$$O_{2(g)} + * = O_2*, \qquad k_{O_2,a}c_{O_2}\theta_V, \qquad [4]$$

$$O_2* \rightarrow O_{2(g)} + *, \quad k_{O_2,d}\theta_{O_2}, \qquad [5]$$

where $k_{O_2,a}$ and $k_{O_2,d}$ are rate constants for adsorption and desorption of molecular oxygen. This molecularly adsorbed oxygen then dissociates irreversibly:

$$O_2* + * \rightarrow 2O*, \quad k_O\theta_{O_2}\theta_V. \qquad [6]$$

This mechanism for oxygen adsorption has been proposed on the basis of a recent TAP study of oxygen adsorption on Pt powder (20). While some caution is needed in extrapolating from transient studies under reduced pressure to steady state kinetic experiments at normal pressures, this mechanism of O_2 adsorption via a molecular precursor state seems entirely plausible. Applying the stationary state approximation to reactions [4]–[6] to obtain an expression for θ_{O_2}, and then substituting this into Eq. [6] gives an expression for the rate of oxygen adsorption:

$$\text{Rate of O adsorption} = \frac{2k_O k_{O_2,a}c_{O_2}\theta_V^2}{k_{O_2,d} + k_O\theta_V}. \qquad [7]$$

Under conditions of high coverage by atomic oxygen, it is assumed that $k_{O_2,d} \gg k_O\theta_V$; i.e., adsorbed molecular oxygen desorbs faster than it dissociates. Thus Eq. [7] becomes

$$\text{Rate of O adsorption} = \frac{2k_O k_{O_2,a}c_{O_2}\theta_V^2}{k_{O_2,d}}. \qquad [8]$$

Finally, NO and NO_2 are presumed to adsorb molecularly and reversibly on the Pt surface,

$$NO_{(g)} + * \leftrightharpoons NO*, \quad K_{NO} = \frac{\theta_{NO}}{c_{NO}\theta_V}, \qquad [9]$$

$$NO_{2(g)} + * \leftrightharpoons NO_2*, \quad K_{NO_2} = \frac{\theta_{NO_2}}{c_{NO_2}\theta_V}, \qquad [10]$$

where K_{NO} and K_{NO_2} are the adsorption coefficients of NO and NO_2, respectively.

Using the steady state approximation for the coverage of oxygen for Eqs. [1]–[3] and [8] gives

$$2k_O K_{O_2}c_{O_2}\theta_V^2 = 25k_{C_8H_{18}}c_{C_8H_{18}}\theta_O\theta_V, \qquad [11]$$

where $K_{O_2} = k_{O_2,a}/k_{O_2,d}$.

The number of surface sites is assumed to be constant, i.e.,

$$1 = \theta_V + \theta_O + \theta_{O_2} + \theta_{NO} + \theta_{NO_2}. \qquad [12]$$

Combining Eqs. [9]–[12] and assuming θ_{O_2} to be negligible gives

$$\theta_V = \frac{25k_{C_8H_{18}}c_{C_8H_{18}}}{25k_{C_8H_{18}}c_{C_8H_{18}}\left(1 + K_{NO}c_{NO} + K_{NO_2}c_{NO_2}\right) + 2k_O K_{O_2}c_{O_2}} \qquad [13]$$

$$\theta_O = \frac{2k_O K_{O_2}c_{O_2}}{\left(25k_{C_8H_{18}}c_{C_8H_{18}}\left(1 + K_{NO}c_{NO} + K_{NO_2}c_{NO_2}\right) + 2k_O K_{O_2}c_{O_2}\right)}. \qquad [14]$$

Substituting Eqs. [13] and [14] into Eq. [1] gives an expression for the rate of n-C_8H_{18} oxidation by O_2:

$$r_{C_8H_{18}-O_2} = \frac{50k_{C_8H_{18}}^2 c_{C_8H_{18}}^2 k_O K_{O_2}c_{O_2}}{\left(25k_{C_8H_{18}}c_{C_8H_{18}}\left(1 + K_{NO}c_{NO} + K_{NO_2}c_{NO_2}\right) + 2k_O K_{O_2}c_{O_2}\right)^2}. \qquad [15]$$

With the C_3H_8–NO–O_2 reaction NO and NO_2 were found to be in pseudo equilibrium; i.e., the conversion of NO to NO_2 was independent of contact time, indicating that NO_2 was being removed at the same rate as it was formed, but NO and NO_2 were not in thermodynamic equilibrium (14). For this reason, NO and NO_2 in the n-C_8H_{18}–NO–O_2 reaction will also be assumed to be in pseudo equilibrium.

The interconversion between NO and NO_2 and the rates of NO_2 formation from NO, and of NO_2 dissociation to give NO, can be written as

$$NO_{(g)} + O* \rightarrow NO_2*, \qquad k_{NO_2,f}c_{NO}\theta_O, \qquad [16]$$

$$NO_2* \rightarrow NO_{(g)} + O*, \quad k_{NO_2,b}\theta_{NO_2}, \qquad [17]$$

where $k_{NO_2,f}$ and $k_{NO_2,b}$ are rate constants for the forward and back reactions for NO_2 formation. If it is assumed that these reactions are much faster than any reaction of NO or NO_2 to give N_2 and N_2O (i.e., NO and NO_2 are in pseudo equilibrium), application of the stationary state approximation to the NO_2 coverage and substitution of Eq. [10] gives the following expression for c_{NO_2} from which the conversion to NO_2 can be calculated:

$$c_{NO_2} = \frac{k_{NO_2,f}c_{NO}\theta_O}{K_{NO_2}k_{NO_2,b}\theta_V}. \qquad [18]$$

This expression fits the experimental data reasonably well (Figs. 6–8).

With the C_3H_8–NO–O_2 reaction the NO_x reduction was directly proportional to the coverage of NO_2 on the Pt surface. This was interpreted in terms of a mechanism in which NO_2, formed by oxidation of NO on the Pt surface, spills over onto the Al_2O_3 support, where it reacts with hydrocarbon-derived species (14). Given that the kinetics

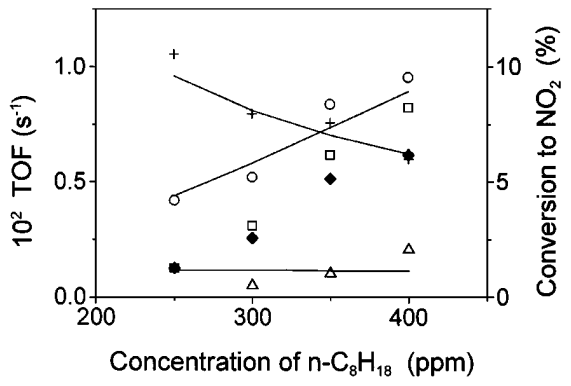

FIG. 8. The effect of varying n-C_8H_{18} concentration on the TOF of n-C_8H_{18} (○), total NO_x (□), NO to N_2 (◆), and NO to N_2O (△), and on conversion of NO to NO_2 (+) for reaction at 200°C over Pt/Al_2O_3 showing fit to low n-C_8H_{18} concentration kinetic model (solid lines). Reactant feed: 500 ppm of NO and 5% O_2.

of n-C_8H_{18} oxidation, NO_2 oxidation, and NO_x reduction at 250 ppm n-C_8H_{18} exhibit the same trends as found with the C_3H_8–NO–O_2 reaction, NO_x reduction might be expected to occur via the same mechanism, and indeed, the rate of deNO_x is satisfactorily fitted in this region: $[C_8H_{18}] \leq$ 250 ppm, $[NO] \leq 1000$ ppm, $[O_2] \leq 10\%$ using

$$r_{NO_x} = k_{NO_x}\theta_{NO_2}. \qquad [19]$$

With the C_3H_8–NO–O_2 reaction attempts were made to fit the rate of NO_x reduction to models based on a considerable number of mechanisms, but only this one was successful (14).

The oxidation of n-C_8H_{18} (or at least species derived from it) by NO_2 needs to be allowed for in the kinetic model for total n-C_8H_{18} oxidation. The overall reactions of NO_2 and n-C_8H_{18} to give N_2 and N_2O are:

$$C_8H_{18(g)} + \frac{25}{2}NO_{2(g)} \rightarrow 8CO_{2(g)} + 9H_2O_{(g)} + \frac{25}{4}N_{2(g)} \qquad [20]$$

$$C_8H_{18(g)} + \frac{50}{3}NO_{2(g)} \rightarrow 8CO_{2(g)} + 9H_2O_{(g)} + \frac{25}{3}N_2O_{(g)}. \qquad [21]$$

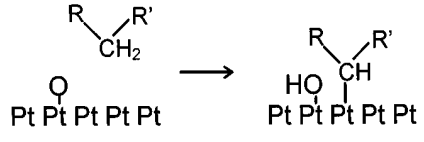

FIG. 9. Schematic representation of the rate-determining step in C_8H_{18} oxidation over a Pt catalyst. The active site consists of two adjacent sites, one of which has an adsorbed O atom on it and the other of which is vacant. R and R′ represent alkyl groups.

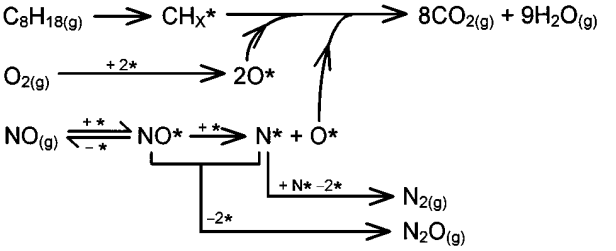

SCHEME 2. Proposed mechanism for the n-C_8H_{18}–NO–O_2 reaction in the high $[C_8H_{18}]/[O_2]$ concentration region. All reactions occur on the Pt surface.

Thus the rate of reaction of n-C_8H_{18} with NO_2 is given by

$$r_{C_8H_{18}-NO_2} = \frac{r_{NO_x}}{5000}\left(300 + S_{N_2}\right), \qquad [22]$$

where S_{N_2} is the percentage selectivity to N_2, ignoring NO_2; i.e.,

$$S_{N_2} = \frac{100n_{N_2}}{n_{N_2} + n_{N_2O}}, \qquad [23]$$

where n_{N_2} and n_{N_2O} are the amounts of N_2 and N_2O formed. The fitted curves in Figs. 6–8 include both the n-C_8H_{18}–O_2 and n-C_8H_{18}–NO_2 reactions (Eqs. [15] and [22]). The curves fit the experimental data reasonably well using the parameters given in Table 1.

Reaction in the Region $[C_8H_{18}] > 500$ ppm, $[NO] \leq 500$ ppm, $[O_2] \leq 5\%$

The n-C_8H_{18}–NO–O_2 reaction behaves similarly to the C_3H_6–NO–O_2 reaction (12) at higher n-C_8H_{18} concentrations ($[C_8H_{18}] > 500$ ppm), provided $[O_2] \leq 5\%$ and $[NO] \leq$ 500 ppm, suggesting that the mechanism of these reactions is similar. The proposed mechanism is summarised in Scheme 2 (compare with (12)).

n-C_8H_{18} oxidation was found to exhibit a high order in O_2 (1.4) and to be zero order in n-C_8H_{18} (Figs. 2 and 4), suggesting that the coverage of oxygen on the Pt surface is small, while that of n-C_8H_{18}-derived species is close to saturation. Thus a plausible mechanism involves n-C_8H_{18} adsorbing and cracking irreversibly on a reduced Pt surface to form various carbonaceous species (CH_x). As before, oxygen adsorbs according to reactions [4]–[6], and the rate of oxygen adsorption is given by Eq. [7]. Under conditions of negligible oxygen coverage, it is expected that $k_{O_2,d} \ll k_O\theta_V$; i.e., molecularly adsorbed oxygen dissociates faster than it desorbs. Thus, the rate of oxygen adsorption becomes

$$\text{Rate of O adsorption} = 2k_{O_2,a}c_{O_2}\theta_V. \qquad [24]$$

The adsorbed oxygen atoms then rapidly react with the adsorbed carbonaceous species to form CO_2 and H_2O. The high order in O_2 can be explained as follows. Increasing the O_2 concentration increases the rate at which carbonaceous

species are burnt off, resulting in a reduction in the coverage of CH_x species and a corresponding increase in the number of vacant sites at which oxygen can adsorb. Thus the order of n-C_8H_{18} oxidation is considerably greater than unity.

A number of models were used to try to describe the adsorption and cracking of n-C_8H_{18}. In these models the dissociative adsorption of the n-C_8H_{18} occurred either via homolytic C–H bond breaking onto two surface sites or via heterolytic C–H bond breaking with the hydrogen atom being abstracted by an adsorbed oxygen atom. The cracking of the adsorbed carbonaceous species was then assumed to occur either by dissociation of the adsorbed species onto vacant sites in a series of steps, or by abstraction of H atoms by adsorbed atomic oxygen, again in a series of steps. However, none of these models was capable of fitting the data. Instead, it will be assumed that the coverage of carbonaceous species is given by

$$\theta_C = 1 - Ac_{O_2}^n \quad \text{for } c_{C_8H_{18}} > 500 \text{ ppm}$$
$$\theta_C = 0 \quad \text{for } c_{C_8H_{18}} < 500 \text{ ppm}, \qquad [25]$$

where n and A are constants. A similar expression was used to model the C_3H_6–NO–O_2 reaction [12], except that in that case $n = 1$. This expression predicts that in the absence of O_2 the surface will be completely covered by carbonaceous species and that the coverage of these species will decrease with increasing O_2 concentration. Provided n-C_8H_{18} is present in sufficiently high concentration (e.g., $[C_8H_{18}] \geq 500$ ppm at 200°C), the oxygen coverage is negligible. While Eq. [25] appears to be somewhat arbitrary, it does allow the logical development of expressions which satisfactorily predict the rates of both n-C_8H_{18} oxidation and of NO reduction to N_2 and N_2O in the specified region.

The proposed mechanism for NO_x reduction is via the dissociation of molecularly adsorbed NO on vacant Pt sites, followed by the formation of N_2 and N_2O by the combination of adsorbed N and NO. This mechanism is in agreement with the observation that the ratio of $N_2 : N_2O$ formed is independent of contact time indicating that N_2 and N_2O are formed from parallel routes. It is also our preferred mechanism for the C_3H_6–NO–O_2 reaction, based on our kinetic (12) and TAP studies (9). This mechanism can be represented as

$$NO_{(g)} + * \leftrightharpoons NO*, \qquad K_{NO} = \frac{\theta_{NO}}{c_{NO}\theta_V} \qquad [26]$$

$$NO* + * \rightarrow N* + O*, \quad k_N\theta_{NO}\theta_V = k_N K_{NO} c_{NO} \theta_V^2 \qquad [27]$$

$$N* + N* \rightarrow N_{2(g)} + 2*, \quad k_{N_2}\theta_N^2 \qquad [28]$$

$$N* + NO* \rightarrow N_2O_{(g)} + 2*, \quad k_{N_2O}\theta_N\theta_{NO} = k_{N_2O}K_{NO}c_{NO}\theta_V\theta_N. \qquad [29]$$

Applying the stationary state approximation to θ_N (using Eqs. [27]–[29]) gives

$$0 \approx \frac{d\theta_N}{dt} = k_N K_{NO} c_{NO} \theta_V^2 - k_{N_2O} K_{NO} c_{NO} \theta_V \theta_N - 2k_{N_2}\theta_N^2. \qquad [30]$$

This is a quadratic in θ_N/θ_V the only physically meaningful solution of which is

$$\frac{\theta_N}{\theta_V} = \frac{-k_{N_2O}K_{NO}c_{NO} + \sqrt{\left(k_{N_2O}K_{NO}c_{NO}\right)^2 + 8k_{N_2}k_N K_{NO} c_{NO}}}{4k_{N_2}}. \qquad [31]$$

The number of surface sites is assumed to be constant, i.e.,

$$1 = \theta_V + \theta_{NO} + \theta_N + \theta_C. \qquad [32]$$

Note that, provided the concentration of n-C_8H_{18} is sufficiently high, the coverage of oxygen is believed to be negligible (see above) and, hence, does not appear in Eq. [32]. Substituting in Eqs. [25] and [26] gives

$$\theta_V = \frac{Ac_{O_2}^n}{1 + K_{NO}c_{NO} + \theta_N/\theta_V} \quad \text{for } c_{C_8H_{18}} > 500 \text{ ppm}. \qquad [33]$$

The rate of the deNO_x reaction is the rate at which NO is converted into N_2 and N_2O (Eqs. [28] and [29]), i.e.,

$$r_{NO_x} = 2k_{N_2}\theta_N^2 + 2k_{N_2O}\theta_N\theta_{NO}. \qquad [34]$$

Substituting in Eqs. [26] and [33] gives

$$r_{NO_x} = \frac{2A^2(\theta_N/\theta_V)c_{O_2}^{2n}\left(k_{N_2}(\theta_N/\theta_V) + k_{N_2O}K_{NO}c_{NO}\right)}{(1 + K_{NO}c_{NO} + \theta_N/\theta_V)^2} \quad \text{for } c_{C_8H_{18}} > 500 \text{ ppm}. \qquad [35]$$

The term in θ_N has been left as θ_N/θ_V rather than substituting in Eq. [31] for simplicity.

Since adsorbed oxygen does not desorb and 25 O atoms are required to totally combust one n-C_8H_{18} molecule, the rate of n-C_8H_{18} oxidation is given (using Eqs. [24] and [27]) by

$$r_{C_8H_{18}} = \left(2k_{O_2,a}c_{O_2}\theta_V + k_N K_{NO} c_{NO}\theta_V^2\right)/25. \qquad [36]$$

Substituting in Eq. [33] gives

$$r_{C_8H_{18}} = \frac{1}{25}\left(\frac{2k_{O_2,a}Ac_{O_2}^{n+1}}{(1 + K_{NO}c_{NO} + \theta_N/\theta_V)} + \frac{k_N K_{NO} A^2 c_{NO} c_{O_2}^{2n}}{(1 + K_{NO}c_{NO} + \theta_N/\theta_V)^2}\right) \quad \text{for } c_{C_8H_{18}} > 500 \text{ ppm}. \qquad [37]$$

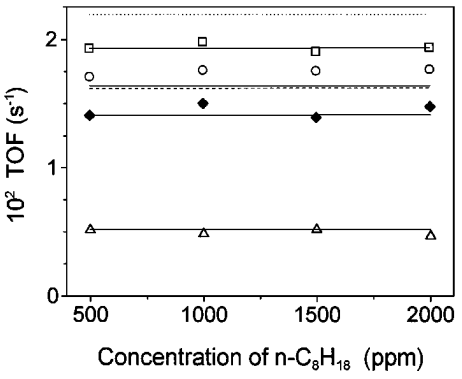

FIG. 10. The effect of varying n-C_8H_{18} concentration on the TOF of n-C_8H_{18} (○), total NO_x (□), NO to N_2 (◆), and NO to N_2O (△) for reaction at 200°C over Pt/Al_2O_3 showing fits to high [C_8H_{18}]/[O_2] concentration kinetic models for NO_x reduction via NO dissociation (solid lines) and by reaction between adsorbed NO and carbonaceous species (dotted lines: short dots NO_x, long dots n-C_8H_{18}). Reactant feed: 500 ppm NO and 5% O_2.

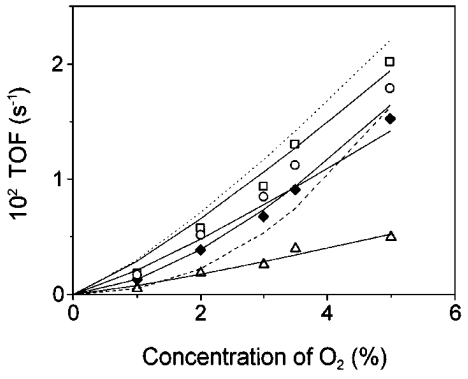

FIG. 12. The effect of varying O_2 concentration on the TOF of n-C_8H_{18} (○), total NO_x (□), NO to N_2 (◆), and NO to N_2O (△) for reaction at 200°C over Pt/Al_2O_3 showing fits to high [C_8H_{18}]/[O_2] concentration kinetic models for NO_x reduction via NO dissociation (solid lines) and by reaction between adsorbed NO and carbonaceous species (dotted lines: short dots NO_x, long dots n-C_8H_{18}). Reactant feed: 1000 ppm n-C_8H_{18} and 500 ppm NO.

These rate equations satisfactorily fit the experimental data (Figs. 10–12, solid line) using the parameters given in Table 2.

A number of other mechanisms have been proposed for the reduction of NO_x under lean-burn conditions. These were summarised in the Introduction. However, none of these other mechanisms was capable of fitting the experimental data. A mechanism involving NO_2 formation seems unlikely for the concentration region under consideration as no NO_2 formation is observed. Mechanisms involving reaction of NO with hydrocarbon derived species, isocyanate formation, and carbonaceous species assisted NO dissociation all involve reaction between carbonaceous species and NO on the Pt surface. The rate of NO_x reduction occurring by one of these mechanisms is expected to be given by

$$r_{NO_x} = k_{NO_x}\theta_C\theta_{NO}. \quad [37]$$

However, this equation was unable to fit the data (Figs. 10–12, dotted lines); in particular, this model predicts the rate of NO_x reduction to be zero order in NO, rather than being inhibited by NO. Thus, these mechanisms can be ruled out.

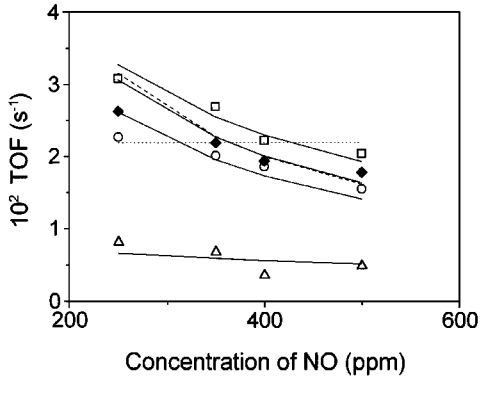

FIG. 11. The effect of varying NO concentration on the TOF of n-C_8H_{18} (○), total NO_x (□), NO to N_2 (◆), and NO to N_2O for reaction at 200°C over Pt/Al_2O_3 showing fits to high [C_8H_{18}]/[O_2] concentration kinetic models for NO_x reduction via NO dissociation (solid lines) and by reaction between adsorbed NO and carbonaceous species (dotted lines: short dots NO_x, long dots n-C_8H_{18}). Reactant feed: 1000 ppm n-C_8H_{18} and 5% O_2.

It is possible to extend this model to allow the effect of temperature on activity to by predicted by allowing the rate constants and adsorption coefficient to vary with temperature (according to the Arrhenius equation and the Van t'Hoff isochore) and by allowing for the concentration gradient along the catalyst bed, as was done with the model for the C_3H_6–NO–O_2 reaction [12]. This predicts the NO_x conversion to have a maximum coincident with 100% hydrocarbon conversion being reached. The reasons for this have been discussed elsewhere (12), and therefore will not be repeated here.

Reaction in Other Concentration Regions

Finally, there exist other concentration regimes in which the kinetics are intermediate between those of the two regions already discussed. In the first region ([C_8H_{18}] ≤ 250 ppm, [NO] ≤ 1000 ppm, [O_2] ≤ 10%) the coverage of oxygen is high, resulting in NO_2 production and inhibition of n-C_8H_{18} oxidation by O_2. In addition NO_x reduction appears to occur on the Al_2O_3 resulting in the kinetics of n-C_8H_{18} oxidation and NO_x reduction being different; e.g., n-C_8H_{18} oxidation is inhibited by NO and O_2, while NO_x reduction is zero order in NO and O_2. In the second region ([C_8H_{18}] > 500 ppm, [NO] ≤ 500 ppm, and [O_2] < 5%), the coverage of carbonaceous species is high and the coverage

of oxygen negligible, resulting in no NO_2 formation and n-C_8H_{18} oxidation having a high order in O_2. NO_x reduction appears to occur via NO dissociation on the Pt surface, resulting in n-C_8H_{18} oxidation and NO_x reduction having comparable kinetics in this region, e.g. both reactions are zero order in n-C_8H_{18}, inhibited by NO and are enhanced by O_2.

There also exist two other regions ($250 < [C_8H_{18}] <$ 500 ppm and $[C_8H_{18}] > 500$ ppm, $[NO] > 500$ ppm, $[O_2] >$ 5%), where the kinetics appear to be intermediate between the first two cases.

First, the $250 < [C_8H_{18}] < 500$ ppm region will be discussed. The model for 250 ppm n-C_8H_{18} is capable of fitting data for the rate of n-C_8H_{18} oxidation and the conversion of NO to NO_2 when the n-C_8H_{18} concentration is varied in the region $250 \leq [C_8H_{18}] < 500$ ppm. However, it does not predict the variation in the rate of NO_x reduction in this region (Fig. 8); the proposed model predicts the rate of NO_x reduction to be zero order in n-C_8H_{18}, while the experimental value is about fourth order. This suggests that under these conditions the mechanism for NO_x reduction is more complicated.

It is notable that the rate of NO_x reduction follows the rate of n-C_8H_{18} oxidation when the n-C_8H_{18} concentration is varied. This behaviour is typical of NO_x reduction occurring via NO dissociation on the Pt surface rather than NO_x reduction occurring on the Al_2O_3 (see above). Therefore, a possible explanation is that the system does not switch sharply from one mechanism to other, but rather that the change is gradual as the n-C_8H_{18} concentration is increased from 250 to 500 ppm. At 250 ppm n-C_8H_{18}, NO_x reduction occurs predominantly on the support. As the n-C_8H_{18} concentration is increased NO_x reduction on the Pt becomes more important, while the coverage of oxygen on the Pt is still sufficient for n-C_8H_{18} and NO_2 oxidation kinetics to be as predicted by the first model. This changing of dominant mechanism explains the very high order of NO_x reduction in n-C_8H_{18}.

In the final region ($[C_8H_{18}] > 500$ ppm, $[NO] > 500$ ppm, and $[O_2] > 5\%$), NO_2 formation and inhibition of n-C_8H_{18} oxidation by O_2 is observed, indicating the presence of oxygen on the Pt surface (as with the first region), and yet n-C_8H_{18} oxidation and NO_x reduction exhibit similar kinetics (i.e., both reactions are inhibited by NO and O_2) which is consistent with NO_x reduction occurring via NO dissociation on the Pt surface (like the second region). It is possible that the behaviour of the system in this region is intermediate between the first two cases because there are either different Pt particles in the catalyst exhibiting behaviour of one or other of the first two regions and/or that the two types of behaviour occur on different regions of the same Pt particle. Alternatively, the third type of behaviour may be a "true" kinetic regime in which there is a high enough coverage of oxygen on the Pt surface to cause NO_2 production and inhibition of n-C_8H_{18} oxidation, but there is not such a high coverage to prevent NO_x reduction occurring via NO dissociation.

5. CONCLUSIONS

The kinetics of the n-C_8H_{18} oxidation reaction appear to be delicately balanced between two kinetic regimes (Schemes 1 and 2). At low $[C_8H_{18}]/[O_2]$, there is insufficient n-C_8H_{18} to remove the adsorbed oxygen from the Pt surface, and, hence, the coverage of oxygen is high, while that of n-C_8H_{18}-derived species is negligible. The high coverage of oxygen results in the production of NO_2. At higher $[C_8H_{18}]/[O_2]$, the n-C_8H_{18} is able to remove almost all the oxygen from the metal surface and the surface becomes saturated with n-C_8H_{18}-derived species. Hence, in this region the n-C_8H_{18} oxidation is zero order in n-C_8H_{18} and no NO_2 formation is observed. The transition from high oxygen coverage to high carbonaceous species coverage is believed to be rather sharp. The state of the Pt surface affects the mechanism of NO_x reduction. The local reducing conditions found on the Pt surface when the coverage of n-C_8H_{18}-derived species is high favours NO_x reduction via NO dissociation on the Pt. In contrast, a high oxygen coverage inhibits NO dissociation, but appears to favour NO_x reduction via reaction on the Al_2O_3 surface between n-C_8H_{18}-derived species and spilt-over NO_2, produced by oxidation of NO on the Pt. The transition between these two mechanisms for NO_x reduction appears to be more gradual than that between the two regimes of n-C_8H_{18} oxidation.

For practical applications, the high $[C_8H_{18}]/[O_2]$ region is the most useful of the two kinetic regimes since the NO_x conversion is much higher. By adding just sufficient reductant upstream of the catalyst to reach the region in which the reaction is zero order in hydrocarbon concentration the maximum NO_x conversion can be achieved for minimum reductant consumption.

ACKNOWLEDGMENTS

We are grateful for financial support for this work from the European Community through Grant EVSV-CT94-0535 and EPSRC Grant GR/K01452.

REFERENCES

1. Taylor, K. C., *Catal. Sci. Technol.*, 5 (1984).
2. Obuchi, A., Ohi, A., Nakamura, M., Ogata, A., Mizuno, K., and Ohuchi, H., *Appl. Catal. B* **2**, 71 (1993).
3. Zhang, G., Yamaguchi, T., Kawakami, H., and Suzuki, T., *Appl. Catal. B* **1**, L15 (1992).
4. Naito, S., and Tanimoto, M., *Chem. Lett.*, 1935 (1993).
5. Tanaka, T., Okuhara, T., and Misono, M., *Appl. Catal. B* **4**, L1 (1994).
6. Obuchi, A., Ogata, A., Takahashi, H., Oi, J., Bamwenda, G. R., and Mizuno, K., *Catal. Today* **29**, 103 (1996).

7. Sasaki, M., Hamada, H., Kintaichi, Y., and Ito, T., *Catal. Lett.* **15**, 297 (1992).
8. Bamwenda, G. R., Obuchi, A., Ogata, A., and Mizuno, K., *Chem. Lett.*, 2109 (1994).
9. Burch, R., Millington, P. J., and Walker, A. P., *Appl. Catal. B* **4**, 65 (1994).
10. Burch, R., and Watling, T. C., *Catal. Lett.* **37**, 51 (1996).
11. Inaba, M., Kintaichi, Y., and Hamada, H., *Catal. Lett.* **36**, 223 (1996).
12. Burch, R., and Watling, T. C., *in* "Proceedings of Fourth International Congress on Catalysis and Automotive Pollution Control, Brussels, April 1997," in press.
13. Burch, R., and Watling, T. C., *Catal. Lett.* **43**, 19 (1997).
14. Burch, R., and Watling, T. C., *J. Catal.* **169**, 45 (1997).
15. Engler, B. H., Leyrer, J., Fox, E. S., and Ostgathe, K., *in* "Catalyst and Automotive Pollution Control III" (A. Frennet and J-M. Bastin, Eds.), *Stud. Surf. Sci. Catal.*, Vol. 96, p. 529. Elsevier, Amsterdam, 1995.
16. Hamada, H., Kintaichi, Y., Sasaki, M., and Ito, T., *Appl. Catal.* **75**, L1 (1991).
17. Burch, R., and Hayes, M. J., *J. Mol. Catal.* A **100**, 13 (1995).
18. Burch, R., Urbano, F. J., and Loader, P. K., *Catal. Today* **27**, 243 (1996).
19. Engel, T., and Ertl, G., *Adv. Catal.* **28**, 1 (1979).
20. Huinink, J., Ph.D. thesis, Chap. 5, Technical University of Eindhoven, The Netherlands, 1995.